Microchemical Journal 219 (2025) 116112

Contents lists available at ScienceDirect

Microchemical Journal

journal homepage: www.elsevier.com/locate/microc

Aptamer-based QCM-D platform for monitoring biofertilizers in soil

Francesco Lunardelli [b,c], Andrea Manfredini [d], Loredana Canfora [d], Mariacristina Gagliardi [a], Matteo Agostini [b], Domenica Convertino [c], Stefano Mocali [g], Eligio Malusa [e,f], Marco Cecchini [a,c,*]

[a] NEST, Istituto Nanoscienze-CNR, Piazza San Silvestro 12, 56126 Pisa, Italy
[b] INTA S.R.l., Intelligent Acoustics Systems, Via Nino Pisano 14, 56122, Pisa, Italy
[c] NEST, Scuola Normale Superiore, Piazza San Silvestro 12, 56126 Pisa, Italy
[d] Council for Agricultural Research and Economics – Center for Agriculture and Environment, Via Della Navicella 4, 00184 Roma, Italy
[e] The National Institute of Horticultural Research, Konstytucji 3 Maja 1-3, 96-100 Skierniewice, Poland
[f] Council for Agricultural Research and Economics – Center for Viticulture and Enology, Via Micca 35, 14100 Asti, Italy
[g] Council for Agricultural Research and Economics – Center for Agriculture and Environment, Via Di Lanciola, 50023 Florence, Italy

ARTICLE INFO

Keywords:
QCM-D
Aptasensor
Biofertilizer monitoring
Soil microbial analysis
Acoustic wave biosensor
Soil extraction

ABSTRACT

The increasing use of bioinoculants to enhance soil quality and crop productivity requires efficient sensor platforms for fast monitoring. EU and national registration demand analytical methods to evaluate environmental fate and long-term effectiveness. Addressing these challenges requires evaluating bioinoculant persistence and impact on microbial communities, emphasizing the need for reliable detection methods in soil.

This study presents an innovative aptamer-based sensing platform using Quartz Crystal Microbalance with Dissipation monitoring (QCM-D) to detect microbial inoculants in soil extract, establishing the basis for portable sensors. The QCM-D platform is functionalized with single-stranded DNA (ssDNA) aptamers specifically designed to detect *Bacillus subtilis* strains. Specificity and selectivity are evaluated using inactivated *B. subtilis* in buffer and compared with negative controls (*P.protegens* and mixed samples).

One aptamer exhibits outstanding specificity, producing a statistically significant distinction between positive and negative controls ($p = 0.019$) with a limit of detection (LoD) between 10^5 and 10^6 CFU/ml.

To validate performance in real matrices, the platform is applied to inoculated soils. Two distinct soils are tested: sandy soil from Poland (neutral pH) and sandy loam from Germany (sub-alkaline pH). An optimized bacterial extraction method yields QCM-D-compatible samples, revealing an average persistence rate of approximately 72 %. In Polish soil, *B. subtilis* generates a response significantly different from controls ($p = 0.0002$), while in German soil differences between *B. subtilis* and *P. protegens* are also significant ($p = 0.04$).

QCM-D analysis demonstrates significant specificity in both soils, as confirmed by triplicate experiments, supporting the aptasensor's robustness and potential for on-site monitoring of microbial inoculants in complex soil matrices.

1. Introduction

The increased interest in bioinoculants for promoting soil health and crop productivity reflects a shift toward more sustainable agricultural practices [1,2]. Bioinoculants, including biofertilizers and biopesticides, are increasingly viewed as alternatives to chemical inputs, contributing to reduced environmental impact in line with EU policies such as the Green Deal and the Farm to Fork strategy [3]. However, broader adoption is hampered by uncertainties surrounding the efficacy and persistence of these microbial agents in soil, as well as their interactions with native soil microbiota [4].

These challenges highlight the need for precise and efficient tools capable of detecting and monitoring bioinoculants within complex matrices such as soil, providing insights into the ecological behavior of bioinoculants and their long-term effects on soil quality and plant productivity.

Traditional detection methods, such as culture-based assays, microscopy-based techniques and DNA amplification techniques (PCR)

* Corresponding author at: NEST, Istituto Nanoscienze-CNR, Piazza San Silvestro 12, 56126 Pisa, Italy.
E-mail address: marco-cecchini@cnr.it (M. Cecchini).

https://doi.org/10.1016/j.microc.2025.116112
Received 13 May 2025; Received in revised form 28 October 2025; Accepted 6 November 2025
Available online 9 November 2025

[5], though effective, are often labor-intensive, costly, and not suited for field-based monitoring. In response, recent research has focused on developing biosensors that offer rapid, sensitive, and selective detection capabilities in complex environments [6,7]. Among these, aptamer-based sensors are particularly promising due to their high specificity, thermal stability, and flexible structure, making them suitable for detecting microbial targets without any need to extract nucleic acids, resulting in minimal sample processing [8,9].

Our goal is to harness the potential of aptamer-based detection and combine it with sensitive platforms to create automated and portable detection systems for microbial inoculants in soil extracts. In this context, the work by Manfredini et al. represents a significant advancement. They successfully isolated, selected, and characterized single-stranded DNA (ssDNA) aptamers to detect a specific *Bacillus subtilis* strain (PCM/B 00105) [10]. The genus Bacillus encompasses several well-known plant-growth-promoting bacteria (PGPB) species, including species widely marketed for their roles in enhancing plant protection, vigor, nutrient uptake, and stress resilience [11,12]. *Bacillus subtilis, in particular, besides playing a key role in conferring biotic and abiotic stress tolerance to several plant species through a variety of mechanisms, is also involved in diverse processes that can promote soil health* [13]. Therefore, the possibility of monitoring and tracking a species or strain belonging to this genus can substantially impact the optimisation of the bioinoculum applications.

Two ssDNA aptamers, named APT1 and APT2 (EU patent application EP4365292), were synthesized and demonstrated high affinity and specificity for *B. subtilis* strains, with dissociation constant (Kd) values in the nanomolar range and a maximum binding intensity (Bmax) of approximately 1. Validation of these aptamers was conducted on three types of inoculated soils with distinct chemical and physical characteristics.

In this study, we combined the detection properties of APT1 and APT2 with a gravimetric sensor based on acoustic wave technology: Quartz Crystal Microbalance with Dissipation monitoring (QCM-D). The sensitive element that we used was an AT-cut quartz crystal positioned between two circular electrodes of gold. Applying an RF voltage across the electrodes induces shear stress within the crystal via the piezoelectric effect. When the applied frequency matches the resonance frequency (set by the crystal's thickness) a bulk acoustic wave (BAW) with shear polarization is generated. Monitoring the resonance frequency (and its specific overtones) is the key element in QCM-D detection. [14,15] According to Sauerbrey, under certain conditions (rigid, evenly distributed, and thin layers), there is a linear relationship between the resonance frequency shift of an oscillating quartz crystal and the mass changes on its surface. By exploiting this mass loading effect, it is possible to gather information on surface mass adsorption by recording the resonance frequency shift. [16] QCM-D monitors both frequency and the dissipation (D) of the acoustic wave to analyze surface layers. The D-value indicates the energy loss during the oscillation of the quartz crystal when interacting with a sample. A low dissipation value indicates minimal energy loss, meaning the layer behaves as rigid (ideal conditions for the Sauerbrey equation). A high dissipation value suggests significant energy loss, often due to viscoelastic behavior, uneven layers, or interactions with a viscous medium. In those conditions, the D-value supports alternative models to determine mass, thickness, and viscoelastic properties. Coupling these properties with a suitable surface functionalization of the quartz crystal enables the QCM-D to function effectively as a sensing technology. [17] There are important works that explore the potential of QCM-D in different fields, such as agrifood [18], medical diagnosis [19] and biomedical [20,21,22].

In recent years, the unique properties of aptamers and their ability to be immobilized on functionalized matrices have been proposed for the development of nanomaterial-based sensitive platforms (aptasensors) for the detection of microbial inocula. For example, aptasensors have been published for the detection of organic pollutants in environmental and biological samples, contaminants in water and soil, and food contamination in food and soil samples [23–25]. These types of aptasensors primarily employ sensing technologies such as electrochemical, optical, and colorimetric transducers. In this context, the integration of an aptasensor based on acoustic wave technology for quantification of bioinocula in soil extracts represents, to the best of our knowledge, an original approach. Unlike culture-dependent methods or molecular assays, this platform enables fast, label-free, and real-time detection of microbial inoculants directly in complex samples. The aptamer-functionalized QCM-D biosensor not only provides continuous monitoring of inoculant persistence but also could offer a unique tool to support sustainable agriculture, optimize fertilizer application, and prevent commercial fraud. By delivering on-site, data-driven analyses, this technology paves the way for improved soil fertility management and enhanced crop yields, ultimately establishing a new paradigm for environmental monitoring and agronomic decision-making.

The present work examines the sensitivity, specificity, and selectivity of QCM-D quartz sensors functionalized with the APT 1 and APT 2 specifically targeting the *B. subtilis* strain (PCM/B 00105). Initial screening identified the most promising aptamer by analyzing inactivated *B. subtilis* samples (positive control) and *P. protegens* (negative control) in a clean buffer. The best-performing aptamer was then evaluated in detecting a real sample, comprising an extract from soil inoculated with various bacterial strains. An extraction protocol was carefully developed to ensure compatibility with the QCM-D microfluidic system. Additionally, tests were conducted on two distinct soil types, Polish and German, to assess performance under varying conditions.

2. Material and methods

2.1. Reagents

Water, sodium carbonate (≥99.5 % purity), and sodium bicarbonate (≥99.5 % purity) were sourced from Sigma Aldrich (St. Louis, MO, USA), while absolute anhydrous ethanol was obtained from Carlo Erba Reagents (Milan, Italy). 1,4-Dithiothreitol (DTT) was used as reducing agent for thiolated molecules (Sigma Aldrich, St. Louis, MO, USA); 11-mercapto-undecanoic acid (11-MUA, Mw 218.4 Da), 11-mercapto-1-undecanol (11-MUD, Mw 204.4 Da) as linker and spacers for probes (Sigma Aldrich); bovine serum albumin (BSA, Mw 66.5 kDa) as blocking proteins (Sigma Aldrich); N-(3-Dimethylaminopropyl)-N0-ethylcarbodiimide hydrochloride (EDCl) and 2,3,5,6-Tetrafluorophenol (TFP) as coupling agents (Sigma Aldrich, purity degree >98 %). Phosphate-buffered saline (PBS, Merck Millipore, Burlington, MA, USA) was used as a buffering solution for the preparation and stabilization of inactivated bacterial samples. Binding buffer (Thermo Fisher Scientific Inc., Waltham, MA, USA) was used as a medium for resuspending bacterial cells and facilitating the interaction with the initial ssDNA during the binding process. Sodium hydroxide solution (NaOH, 200 mM) was used to treat the bound ssDNAs, enabling the recovery of single-stranded DNA (ssDNA) in the supernatant. Tryptic soy agar (TSA, Merck KGaA, Darmstadt, Germany) was used as a culture medium. Sodium pyrophosphate (Merck KGaA, Darmstadt, Germany) and Tween 20 (Merck KGaA, Darmstadt, Germany) were used as components of the extracting solution.

2.2. Bacterial isolation

Bacterial strains have been isolated at the National Institute of Horticultural Research (Skierniewice, Poland) and maintained in the SYMBIO BANK of the Institute.

The *B. subtilis* strain PCM/B 00105 was cultured in phosphate-buffered saline (PBS) and isolated through serial dilution up to a dilution of 10^{-7}. The diluted samples were plated in duplicates on Trypticase Soy Agar (TSA) (Thermo Fisher Scientific Inc., Oxoid Ltd., Basingstoke, U.K.) and incubated at 30 °C for a period of 24 to 48 h.

The *Pseudomonas protogens* strain was cultivated on nutrient agar medium (Thermo Fisher Scientific Inc., Oxoid Ltd., Basingstoke, U.K.), incubated at 30 °C for 24 h.

2.3. Aptamer selection

The SELEX process for selecting suitable aptamers utilized a random single-stranded DNA (ssDNA) library along with PCR primers [10] The ssDNA library consisted of a 40-nucleotide randomized region, flanked by approximately 20-nucleotide primer regions, forming an 84-nucleotide oligonucleotide. A biotin-modified reverse primer was employed in the STC-SELEX process [26]. *Bacillus subtilis* PCM/B 00105 was cultured overnight and then subcultured to reach about 1×10^8 CFU/ml. These cultured bacteria were washed with PBS and resuspended in a binding buffer. The initial ssDNA library (100 pmol) was mixed with 10^{-7} bacterial cells in a binding buffer and incubated for 1 h at room temperature. Unbound ssDNA was washed off, while bound ssDNA was recovered by centrifugation and heat treatment. The ssDNA was filtered using centrifugal filter units to remove impurities and its purity was assessed by checking the 260/280 nm absorbance ratio. The elution yield was calculated before and after binding using a spectrophotometer (Nanodrop1000 Thermo Fisher Scientific Inc., Waltham, MA, USA). The recovered ssDNA was amplified via PCR with unmodified forward and biotin-modified reverse primers. PCR products were purified, and ssDNAs were isolated from double-stranded DNA (dsDNAs) using streptavidin-coated magnetic beads (Thermo Fisher Scientific Inc., Waltham, MA, USA). The bound ssDNAs were treated with NaOH to recover ssDNA in the supernatant, purified again, and used for the second selection round, repeating this process for four rounds. After the final round, the isolated ssDNAs were amplified to obtain dsDNA, cloned using a TOPO TA Cloning Kit, and transformed into *Escherichia coli* DH10B cells. Plasmid DNA was purified from selected colonies, and the presence of inserted fragments was confirmed with restriction enzymes and PCR. The secondary structure of each sequence was predicted using Mfold [27].

2.4. Bacterial inactivation

Bacterial inactivation was performed on two microbial strains, *Bacillus subtilis* and *Pseudomonas protegens*, utilizing heat treatment. Following growth testing on a solid culture medium, 4–5 isolated colonies were resuspended in sterile demineralised water to achieve a bacterial density of 0.5 CFU (McFarland, 1907). The bacterial suspension was then inactivated at 70 °C for 10 min in a Thermal Mixer (Thermo Fisher Scientific Inc., Basingstoke, U.K.) with constant agitation set at 200 rpm. To verify inactivation, 100 µl of the treated mixture was plated onto a TSA culture medium and incubated at 30 °C for 24 h. Microscopic examination further confirmed that the bacterial cells remained intact after treatment.

Subsequently, a solution of 10^9 bacteria per ml was made up in PBS to test the functionalized aptamer detection system on the QCM-D medium.

2.5. Soil microcosm preparation and bacterial inoculation

Microcosms from two distinct soils were prepared to evaluate the effectiveness of the aptamers (for detailed information on the physical and chemical characterisations, please refer to Manfredini et al., 2023). The chemical and physical properties of these soils can be considered representative of various European soils. [28] To assess the efficacy and efficiency of bacterial recovery using aptamers, the soils were sterilised to eliminate potential interference from indigenous microflora. The sterilisation process involved three cycles in an autoclave (121 °C for 30 min), each followed by a 24-h incubation period at room temperature. The success of the sterilisation was confirmed by inoculating TSA culture medium with serial dilutions of the sterilised soil in a physiological solution.

Upon establishing the sterility of the soils, triplicate microcosms were prepared using 2 g of soil, to which 500 µl of bacterial inoculum was added, consisting of a bacterial suspension with a concentration of 10^7–10^8 bacteria per ml. An abiotic control was similarly prepared, but 500 µl of sterile water was added instead of the bacterial inoculum. The microcosms were then incubated for five days at a temperature of 30 °C.

This method is in line with the real-world use case of microbial biofertilizers, which are used to inoculate the soils. The amounts used for the inoculation corresponded to the concentration used for the inoculation of these soils with live *Bacillus subtilis* under field application. The analysis was carried out in authentic soil matrix, and inoculation is intrinsic to the intended field application.

2.6. Bacterial cell extraction from soil microcosm

To facilitate the release of microorganisms from the soil microcosm, 8 ml of an extracting solution (consisting of 0.1 % sodium pyrophosphate *w/v* and 0.05 % Tween 20 *v/v*) was introduced to each soil microcosm. The mixture was then subjected to mechanical shaking at 200 rpm for 30 min at room temperature. Following this, the soil microcosm was allowed to settle for an additional 30 min [29]. An aliquot of the supernatant was subsequently analyzed for bacterial presence using a Thoma-Zeiss hemocytometer chamber (Thoma, 1882) under a 40× magnification optical microscope. The number of cells present in each soil microcosm sample was recorded.

To ensure compatibility with the sensor platform, the extract is left to settle for at least 24 h to allow precipitation. After the settling period, the supernatant is carefully collected and transferred. This supernatant is then prepared for analysis using the designated sensor platform. Fig. S1 in the supplementary materials describes this process.

2.7. Spectrometric profile of soil extracts

To investigate and quantify the differences in the composition of the extracts before and after sedimentation, a UV–Vis spectrophotometric analysis was conducted. The analyses were performed using a JASCO V-550 UV/VIS spectrophotometer (Jasco, Cremella, Italy). The absorbance spectrum was recorded over a wavelength range from 200 to 800 nm Baseline correction was applied using a blank solution prepared with extracting solution to eliminate background noise and ensure the reliability of the results.

2.8. Quartz crystal microbalance with dissipation monitoring experiments

QCM-D (E4 model, Q-Sense AB, Biolin, Sweden) measurements were conducted using AT-cut quartz crystals with gold surfaces. These crystals have a fundamental resonance frequency of 5 MHz, a diameter of 14 mm, and a thickness of 100 nm. The fluidic cells were thermostatted at 25 °C and measurement were performed in static mode (stop flow). The platform enables real-time measurement of the normalized frequency shift ($\Delta F_n/n$) and dissipation variation (ΔD_n) across up to $n = 7$ odd overtones. In this study, the results are presented exclusively for the 3rd, 5th, and 7th overtones, which were selected as the most representative.

To ensure the applicability of the Sauerbrey model, ΔD_n values were checked, adhering to the criterion of $\Delta D_n < 2.0 \times 10^{-6}$ as described in [16].

2.9. Aptasensor functionalization strategy

The functionalization strategy of the gold surface with aptamers is detailed and analyzed in Fig. 1. Specifically, panel a depicts a schematic representation of all the steps of quartz-crystal functionalization (not to scale). The initial step entails the formation of a self-assembled monolayer (SAM), comprising 11-MUA as a linker and 11-MUD as a spacer. The spacer molecule serves to reduce the density of free carboxylic

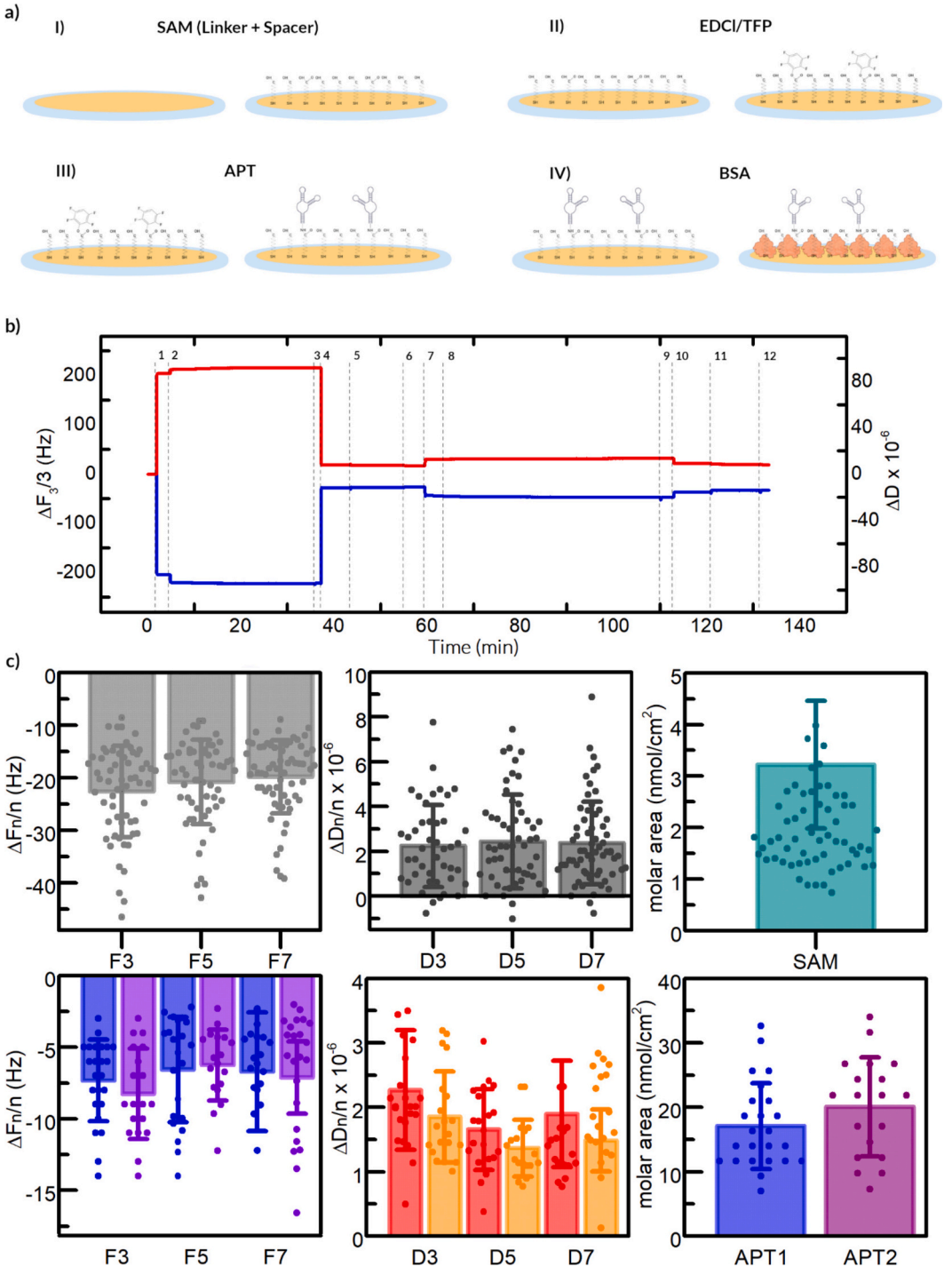

Fig. 1. Functionalization: **Panel a)** Schematic representation of the quartz crystal functionalization (not in scale) showing I) formation of the self-assembled monolayer (SAM) composed of 11-MUA and 11-MUD in the presence of DTT as a reducing agent; II) activation of carboxylic acid groups in the adlayer via EDCI/TFP chemistry; III) aptamer immobilization through reaction between the activated adlayer and an amine group; and IV) application of a blocking solution of BSA to prevent nonspecific binding.

groups while simultaneously enhancing the hydrophilicity of the sensor surface, thereby minimizing nonspecific adsorption [30,31]. The SAM solution is prepared as a 1:1 *v*/v water/ethanol mixture containing 11-MUA and 11-MUD, with an overall solute concentration of 2 mg/ml. The weight percent of 11-MUA to 11-MUD is fixed at 20:80. To this solution, DTT is added in a quantity corresponding to 0.1× mol/mol of free thiols. The incubation period prior to the final rinse is set at 30 min.

Activation of carboxylic acids is accomplished through the use of an aqueous solution containing 0.5 mM of EDCl and 0.5 mM of TFP, incubated for 10 min. This activation method produces tetrafluorophenyl esters that are both more stable and more reactive toward amines, limiting the esterification between 11-MUA and 11-MUD, thereby increasing the efficiency of subsequent conjugation with the bioreceptor. The conjugation reaction is carried out under slightly basic buffered conditions [32].

Aptamer immobilization is achieved via the reaction between the activated adlayer and amine groups. The probe solution consists of aptamers in a carbonate/bicarbonate buffer at a concentration of 100

μg/ml, incubated for 60 min.

The final step involves the injection of blocking solution composed of an aqueous BSA solution at a concentration of 1 mg/ml with an incubation time of 10 min.

2.10. Microscopic analysis of crystals after samples analysis

To support the data obtained via QCM-D, crystals were analyzed using an optical microscope (1/4" CCD color board camera with a 100× microscope objective, Polytec). Images were captured across multiple regions of each crystal to ensure representative sampling, with four images per crystal analyzed using ImageJ software. This approach enabled the estimation of the average bacterial count per unit area. Furthermore, selected portions of the crystals were examined using a high-resolution scanning electron microscope (Zeiss Merlin SEM) to analyze the morphology and dimensions of the immobilized bacteria.

2.11. Data analysis and statistics

The values of ΔFn/n and ΔDn/n are reported, calculated as the difference between the baseline acquired at the start of each measurement step and the post-rinse signals. During the functionalization monitoring phase, both for adlayer adhesion and correct aptamer binding, a series of N replicates were performed, with ΔFn/n (Hz) and ΔDn/n (dimensionless) continuously recorded. The results are presented as the mean of replicates (N), with error bars indicating the standard deviation (SD). The fundamental frequency (ΔF0) was excluded from the analysis due to its high sensitivity to environmental noise, while data related to the 3rd, 5th, and 7th harmonics are presented to ensure reliability and accuracy.

In accordance with the Sauerbrey eq. [16], reported below:

$$\Delta m = -C\frac{\Delta F_n}{n}$$

where C is a constant that depends on the physical characteristics of the crystal, the areal molar mass (mol/cm^2) was calculated as the ratio between the surface mass density and the molecular weight.

In the first step of bacteria detection (clean buffer), 4/5 experiments were conducted for each condition (negative and positive controls) for each aptamer. $\Delta F_n/n$ (Hz) and $\Delta D_n/n$ (dimensionless) were continuously recorded throughout the procedure. The results are presented as the mean of replicates, with error bars indicating the standard deviation. For simplicity, only data from the 3rd overtone were analyzed and reported in this phase.

Lastly, for soil detection, 3 replicates were performed for each condition (abiotic control, negative control, and positive control) for each of the two soil types. As in the previous phase, data were presented considering only the 3rd overtone to maintain consistency and facilitate data interpretation.

Statistical significance was evaluated using non-parametric *t*-tests on the obtained distributions, allowing for robust comparisons between experimental conditions.

2.12. Surface morphology analysis via atomic force microscope (AFM)

Atomic force microscopy (AFM, Dimension Icon, Bruker, Billerica, MA, USA) was carried out in Soft Tapping mode to evaluate surface morphology and estimate roughness of the sensor before and after functionalisation. All measurements were performed in air at room temperature and atmospheric pressure. The acquired data were processed and analyzed using Gwyddion (version 2.67).

3. Results

3.1. Functionalization of QCM-D crystals

We started our analysis by examining the functionalization process of the QCM-D crystals, as outlined in the previous section. Fig. 1, panel b depicts the pattern of the real-time monitoring of frequency and dissipation during the entire functionalization process, using the 3rd overtone as representative. Particular attention was given to the formation of the self-assembled monolayer (SAM) composed of 11-MUA and 11-MUD in the presence of DTT as a reducing agent. Specifically, the frequency shifts and dissipation changes were analyzed for the 3rd, 5th, and 7th harmonics measured after water rinsing, following SAM incubation. Fig. 1, panel c, shows the bar plots of the cumulative signals corresponding to this phase. The frequency shifts across the harmonics are approximately −20 Hz, and the average dissipation changes are close to the threshold value of 2×10^{-6}. Despite the dissipation change values being at the threshold limit of the Sauerbrey model, the molar areal mass was calculated using a molecular weight (mean from 11-MUA and 11-MUD) of 204.7 g/mol, considering only the 3rd harmonic. This resulted in a value of 2.0 ± 0.8 nmol/cm^2. Table 1 summarizes the average values from the entire set of measurements, encompassing all functionalization processes conducted.

To confirm successful aptamer binding and evaluate reproducibility, we analyzed the normalized frequency shifts and dissipation changes after post-rinsing with water following aptamer solution incubation. Fig. 1 (panel c) and Table 1, present the cumulative bar plots and results for APT 1 and APT 2, displaying frequency and dissipation signals. In this case as well, the Sauerbrey conditions were satisfied, allowing for the assumption of rigid adhesion. Specifically, an average frequency shift of approximately −8 was observed, with dissipation changes ranging between 1.4 and 2.3 × 10^{-6}. These results enabled the calculation of the molar areal mass, yielding values of 17 ± 6 pmol/cm^2 for APT 1 and 20 ± 7 pmol/cm^2 for APT 2.

To complete the characterization of the QCM sensor's surface morphology, we performed AFM analysis of the main functionalisation steps; the results are reported in the Supplementary Materials (Fig. S2). AFM reveals a stepwise evolution. Clean Au displays a granular, polycrystalline topography with low phase contrast, consistent with a uniform, low-dissipation metal. SAM formation preserves the grain structure but drives the phase to more negative values with higher contrast; faint, less-negative ridges at grain boundaries suggest locally stiffer regions (exposed Au or compressed/ordered SAM). Aptamer immobilization further increases the negative phase and introduces discrete bright domains. After BSA blocking, filamentous features became evident, exhibiting a brighter phase.

Table 1
Functionalization results.

	SAM		
	3rd	*5th*	*7th*
$\Delta F_n/n$ [Hz]	−23 ± 8	−21 ± 8	−20 ± 7
$\Delta D_n/n$ [x10^6]	2,2 ± 1,8	2,0 ± 2,0	2,4 ± 1,8
	APT 1		
	3rd	***5th***	***7th***
$\Delta F_n/n$ [Hz]	−7 ± 3	−7 ± 4	−7 ± 4
$\Delta D_n/n$ [x10^6]	2,3 ± 0,9	1,6 ± 0,6	1,9 ± 0,8
	APT 2		
	3rd	***5th***	***7th***
$\Delta F_n/n$ [Hz]	−8 ± 3	−6 ± 2	−7 ± 2
$\Delta D_n/n$ [x10^6]	1,8 ± 0,7	1,4 ± 0,4	1,5 ± 0,5

Panel b) Representative QCM-D traces (referenced to overtone 3) showing shifts in frequency (blue line) and dissipation changes (red line). The sensogram highlights the sequential events during the functionalization process, starting with crystal in water: 1 pre-rinsing with water/ethanol, 2 injection of the SAM solution, 3 rinsing with water/ethanol, 4 rinsing with water, 5 injection of the activation solution, 6 rinsing with water, 7 pre-rinsing with carbonate/bicarbonate buffer, 8 injection of the aptamer solution, 9 rinsing with carbonate/bicarbonate buffer, 10 rinsing with water, 11 injection of the blocking solution, and 12 rinsing with water. **Panel c)** SAM and Aptamers detection. Box plots on the first row show the QCM-D signals after SAM monolayer formation, including frequency shifts and dissipation changes for overtones 3, 5, and 7 (post water rinsing after SAM incubation, Step 4). The molar areal mass of the SAM, assuming rigid binding conditions and a molecular weight of 204.7 g/mol, is also reported, considering only the third overtone. Binding APT1 (blue and red) and APT2 (purple and orange): bar plots show the QCM-D signal differences between water rinsing post-activation (Step 6) and post-aptamer incubation (Step 10). Frequency shifts and dissipation changes are reported for overtones 3, 5, and 7, while the molar areal mass is calculated using only overtone 3, with molecular weights of 7601.9 g/mol for APT 1 and 7288.7 g/mol for APT 2.

3.2. QCM-D aptasensor performance for detection of B. subtilis in clean buffer

The performance of the functionalized sensors with APT 1 and APT 2 was assessed using inactivated bacteria in a clean PBS buffer matrix. Initial experiments were conducted to detect *B. subtilis* at a concentration of 10^6 CFU/ml, allowing for an evaluation of sensor response under controlled conditions. To validate the specificity of the detection, additional tests were performed using *P. protegens* as a negative control, applying the same bacterial concentration (10^6 CFU/ml). Furthermore, a mixed solution containing both *B. subtilis* and *P. protegens* at equal concentrations was tested to further assess the selectivity of the aptasensor.

3.2.1. APT 1 performance in clean buffer

For the APT 1 functionalization, representative sensor response traces and cumulative bar plots are presented in Fig. 2. The detection of *B. subtilis* yielded an average frequency shift of -3.3 Hz $\pm$ 0.9 Hz, accompanied by minimal dissipation changes of $(0.3 \times \pm 0.3) \times 10^{-6}$, after the final rinsing phase. This distinct negative frequency shift and minimal dissipation change are distinctly observable in the real-time sensorgram (Fig. 2, panel a). These data highlight the consistency and reliability of the sensor response to *B. subtilis* in clean buffer, demonstrating the robustness of the aptasensor in capturing the target analyte.

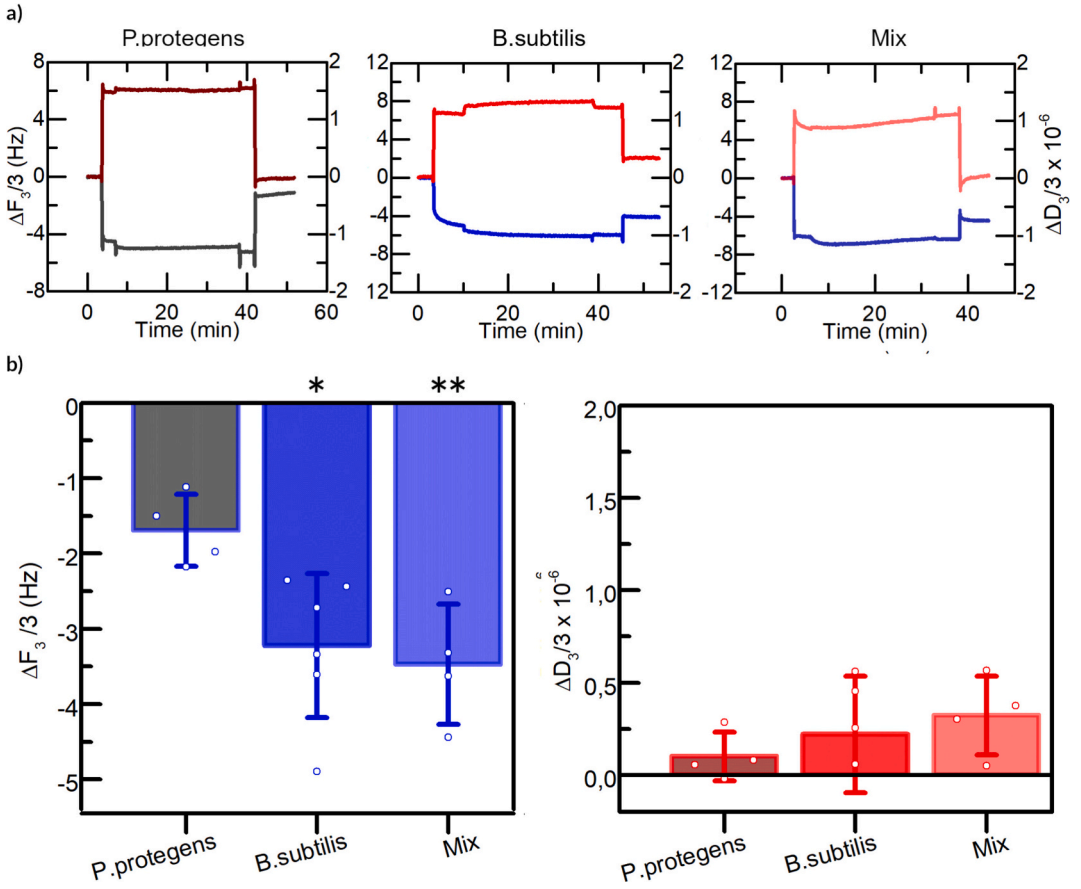

Fig. 2. Performance of the APT1-functionalized biosensor for bacterial detection in clean buffer. **Panel a):** Representative QCM-D traces illustrating frequency shifts and dissipation changes during the detection process in PBS buffer. Sequential events are outlined as follows: (1) functionalized crystal pre-rinsing with PBS, (2) injection of inactivated bacteria sample at a concentration of 1×10^6 CFU/ml, (3) rinsing with PBS, and (4) final rinsing with water. From left to right, the traces correspond to the detection of negative control (*P. protegens*), *B. subtilis* and a sample composed of a mixture of the two bacterial strains. **Panel b):** Cumulative QCM-D frequency and dissipation responses (overtone 3) from multiple replicates for the negative control (*P. protegens*), the positive control (*B. subtilis*), and the mixture of the two strains. Despite the low number of replicates, the distributions passed the normality test, and the data are presented with the mean highlighted. The whiskers indicate the standard deviation. Statistically significant frequency shifts are observed, with a *p*-value of 0.019 for the comparison between *P. protegens* and *B. subtilis*, and 0.009 for the comparison between *P. protegens* and the mixture. The dissipation variations for all samples remain below the threshold of 2×10^{-6}, indicating rigid adhesion in accordance with the Sauerbrey model.

To rigorously assess the specificity of APT 1, additional experiments were conducted using *P. protegens* as a negative control. As shown in the corresponding sensor response bar plot (Fig. 2, panel b), significantly smaller frequency shifts were observed compared to the positive control, with an average shift of −1.7 Hz ± 0.4 Hz and negligible dissipation changes around zero (0.1 ± 0.1) × 10^{-6}, after the final rinsing phase. These results unequivocally demonstrate the lower binding affinity of APT 1 for *P. protegens*, reinforcing the high specificity of the aptasensor for the target *B. subtilis*.

To further substantiate the selectivity of APT 1, a mixture of *B. subtilis* and *P. protegens* at a total concentration of 10^6 CFU/ml was analyzed. The aptasensor response, depicted in the bar plot (Fig. 2, panel b), revealed average frequency shifts of −3.5 Hz ± 0.7 Hz, with dissipation changes remaining consistently close to zero (0.3 ± 0.2) × 10^{-6}, after the final rinsing phase. Notably, a pronounced negative frequency shift is also apparent in the representative real-time signal trace (Fig. 2, panel a). These findings clearly demonstrate that the APT 1 sensor predominantly interacts with *B. subtilis*, even in the presence of *P. protegens*, thereby confirming its high selectivity and reliable performance under competitive conditions.

The entire dataset is reported in Table 2. Statistical analysis using a *t*-test further validated the significance of these findings, yielding a *p*-value of 0.019 for the comparison between the negative control and *B. subtilis*, and a p-value of 0.009 for the comparison between the negative control and the mixture.

3.2.2. APT 2 performance in clean buffer

Following the same experimental framework used for APT 1, the performance of the APT 2 sensor was evaluated using inactivated bacteria in a clean PBS buffer matrix. Representative sensor response traces and cumulative bar plots are presented in Fig. 3. Detection of *B. subtilis* at a concentration of 10^6 CFU/ml resulted in an average frequency shift of −2.3 ± 0.9 Hz, with minimal dissipation changes of (0.4 ± 0.4) × 10^{-6}, after the final rinsing phase. This negative frequency shift and minimal dissipation change are clearly observable in the real-time sensorgram (Fig. 3, panel a). Although the response demonstrated good reproducibility, the signal intensity appeared lower compared to APT 1, indicating a reduced sensitivity of the APT 2 sensor.

The specificity of APT 2 was assessed using *P. protegens* as a negative control. The analysis revealed an average frequency shift of −2.0 ± 0.9 Hz and an average dissipation change of (0.1 ± 0.4) × 10^{-6} (Fig. 3 and Table 2), values closer to those observed for the target bacteria. This outcome highlights a reduced discrimination capacity between *B. subtilis* and *P. protegens* compared to APT 1, suggesting a lower binding specificity of APT 2, likely due to non-specific interactions.

To further evaluate the selectivity of APT 2, a mixed sample containing *B. subtilis* and *P. protegens* at a combined concentration of 10^6 CFU/ml was analyzed. The sensor response, depicted in the bar plot (Fig. 3, panel b), showed an average frequency shift of −3.5 ± 1.2 Hz, with dissipation changes remaining consistently low at (0.2 ± 0.1) × 10^{-6}, after the final rinsing phase. Despite the predominant interaction with *B. subtilis* even in the presence of *P. protegens*, the statistical analysis revealed no significant differences between the frequency shift distributions for the mixed sample and the negative control, indicating a lack of reliable differentiation. In this case, the statistical significance obtained with APT 1 is lost, confirming the reduced reliability of APT 2. The entire dataset is reported in Table 2.

Table 2
Bacteria detection in clean buffer.

	APT 1			APT 2		
	P. protegens	*B. subtilis*	*Mix*	*P. protegens*	*B. subtilis*	*Mix*
$\Delta F_3/3$ [Hz]	−1,7 ± 0,4	−3,2 ± 0,9	−3,5 ± 0,7	−2,0 ± 0,9	−2,3 ± 0,9	−3,5 ± 1,2
$\Delta D_3/3$ [x10^6]	0,1 ± 0,1	0,3 ± 0,3	0,3 ± 0,2	0,1 ± 0,4	0,4 ± 0,4	−0,1 ± 0,5

To further evaluate the aptasensor's performance, additional tests were performed at a lower concentration of 10^5 CFU/ml of *B. subtilis* for both aptamers. As described in the supplementary materials (Fig. S3), the sensor was unable to detect this lower concentration, suggesting a detection limit of about 10^6 CFU/ml.

Microscopic analysis of Crystals functionalised with APT1 and APT2 and loaded with bacterial strains.

To validate the QCM-D signals, the functionalized crystals were examined under an optical microscope after incubation with bacteria to estimate the number of bacterial cells per unit area (U/mm^2), as shown in Fig. S4 of supplementary materials.

For APT 1 functionalization, the bacterial counts were as follows: *P. protegens* = 920 ± 150 U/mm^2, *B. subtilis* = 1660 ± 380 U/mm^2, and the mixture = 1790 ± 290 U/mm^2. For APT 2 functionalization, the bacterial counts were: *P. protegens* = 1050 ± 90 U/mm^2, *B. subtilis* = 2220 ± 790 U/mm^2, and the mixture = 1790 ± 410 U/mm^2.

The results obtained from both aptamers demonstrated a high degree of consistency with the QCM-D analysis, indicating a strong correlation between the two methodologies. This correlation is particularly robust given that the QCM-D frequency shift is directly proportional to the adhered mass, and the bacterial counting method independently confirms this relationship. This complementary approach, based on bacterial counting, reinforces the QCM-D results by directly correlating the observed frequency shift with the mass of adhered cells, thereby providing an independent validation of the sensor's performance. The high level of statistical significance (p-value <0.0001) obtained when comparing both *B. subtilis* to *P. protegens* and the mixed bacteria sample to *P. protegens,*for both APT1 and APT2, further supports the reliability of the results.

3.3. QCM-D aptasensor capability for detecting B. subtilis in soil samples

3.3.1. Inoculation efficiency

Following soil inoculation with the two bacterial strains, bacterial recovery rates were assessed to provide insight into their persistence and viability, allowing for a better understanding of their interaction with the soil matrix and texture and thus about factors that could limit the cells detection and/or extraction. As expected, both strains were not detected in the non-inoculated control samples, confirming the sterility of the soil prior to their inoculation. Likewise, no other bacterial species were found in the tested soil extracts, ensuring that the introduced strains were the only microorganisms present. For inoculated Polish soil samples, the Thoma-Zeiss hemocytometer count revealed bacterial concentrations of 2.0 × 10^6 CFU/ml for *B. subtilis* and 2.8 × 10^7 /ml for *P. protegens*, compared to initial inoculum concentrations of 2.7 × 10^6 /ml and 3.5 × 10^7 /ml, respectively. This resulted in calculated persistence rates of 74.4 % for *B. subtilis* and 80 % for *P. protegens*, indicating a good persistence of bacterial cells in this soil type.

For the German soil, initial inoculum concentrations were measured at 1.7 × 10^6 /ml for *B. subtilis* and 1.5 × 10^7 /ml for *P. protegens*. Following the bacterial release procedure, the recovered concentrations were 1.1 × 10^6 /ml for *B. subtilis* and 1.3 × 10^7 /ml for *P. protegens*, corresponding to recovery rates of 58.8 % and 73.3 %, respectively.

3.3.2. Soil extracts assessment

Before analysis, the samples were extracted to obtain a soil-derived liquid phase compatible with QCM-D microfluidic analysis. The extraction process was optimized through physicochemical characterization, focusing particularly on sedimentation behavior to minimize interference from large particles on the QCM-D sensor surface.

The UV–Vis spectra of the turbid soil extract (green line in Fig. S1) and the extract after sedimentation (blue line in Fig. S1) were analyzed to compare their absorbance profiles and evaluate their compatibility with QCM-D microfluidic analysis. The turbid extract displayed

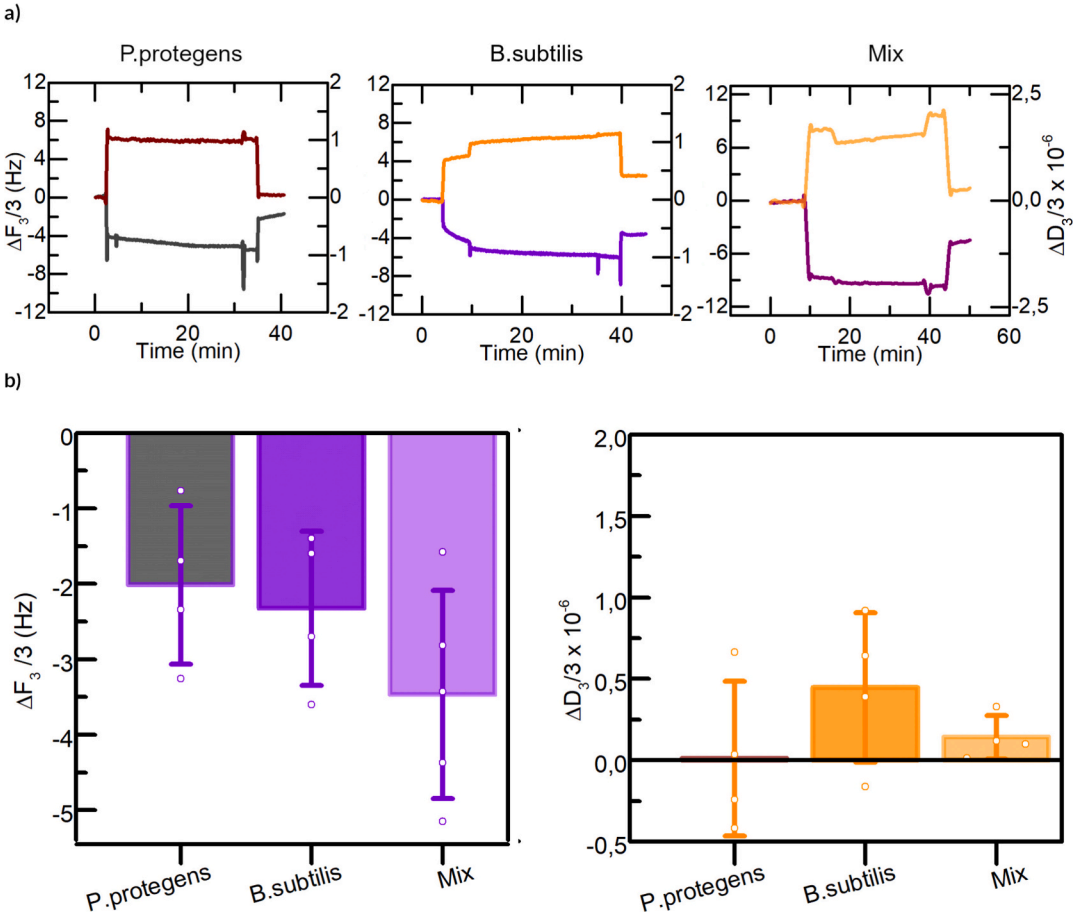

Fig. 3. Performance of the APT 2-functionalized biosensor for bacterial detection in clean buffer. **Panel a):** Representative QCM-D traces illustrating frequency shifts and dissipation changes during the detection process in PBS buffer. Sequential events are outlined as follows: (1) functionalized crystal pre-rinsing with PBS, (2) injection of inactivated bacteria sample at a concentration of 1×10^6 CFU/ml, (3) rinsing with PBS, and (4) final rinsing with water. From left to right, the traces correspond to the detection of negative control (*P. protegens*), *B. subtilis* and a sample composed of a mixture of the two bacterial strains. **Panel b):** Cumulative QCM-D frequency and dissipation responses (overtone 3) from multiple replicates for the negative control (*P. protegens*), the positive control (*B. subtilis*), and the mixture of the two strains. Despite the low number of replicates, the distributions passed the normality test, and the data are presented with the mean highlighted. The whiskers indicate the standard deviation. In this case, it is not possible to achieve statistical significance for the difference among the various distributions of frequency shifts. The dissipation variations for all samples remain below the threshold of 2×10^{-6}, indicating rigid adhesion in accordance with the Sauerbrey model.

consistently high absorbance across the measured wavelength range, with a gradual and slight decrease toward higher wavelengths. In contrast, the extract after sedimentation showed a marked decline in absorbance beyond 400 nm, characterized by a rapid drop at higher wavelengths. This behavior indicates that the remaining fraction was predominantly composed of smaller, less absorbent aggregates or insoluble particles. The separation process effectively isolated the absorbing species within the liquid phase, resulting in a sedimented extract with minimal optical activity and a more defined spectral profile.

3.3.3. Performance of aptasensors with soil extracts

After evaluating and quantifying the performance of the two aptasensors in clean buffer, the APT 1 functionalization was selected for testing in real soil samples. Indeed, in this analysis APT 1 demonstrated superior specificity and selectivity in detecting *B. subtilis with respect to APT2*, while maintaining excellent reproducibility. Furthermore, the values obtained through QCM-D analysis were corroborated by optical microscopy images, reinforcing the reliability of the results. Two types of soil with distinct chemical and physical characteristics were tested: sandy soil with a neutral pH (from Poland) and medium-textured sandy loam soil with a sub-alkaline pH (from Germany). The soil samples were prepared as described in the Materials and Methods section, and the resulting extracts, compatible with the QCM-D microfluidics, were analyzed to assess the performance of the sensor platform.

3.3.4. Polish soil

The first type of soil tested was a Polish soil sample. After completing the inoculum preparation and extraction protocol, the bacterial concentration obtained for analysis was approximately 2×10^6 CFU/ml. Detection experiments were conducted using positive control samples (*B. subtilis*), negative control samples (*P. protegens*), and abiotic control samples (soil extract without inoculation) to evaluate the impact of the soil matrix on the sensor's performance.

Fig. 4 presents the detection results for the Polish soil. Panel a show the real-time traces of frequency shift and dissipation (referred to the 3rd overtone) during *B. subtilis* detection. The traces are well-defined, highlighting the sensor's compatibility with the complex soil matrix.

Panel b, together with Table 3, display the cumulative detection results obtained from three replicates, presented as bar plots to illustrate the mean frequency shifts and dissipation changes for each sample type. For *B. subtilis*, the average frequency shift was -4.2 ± 0.5 Hz, accompanied by a dissipation change of $(0.7 \pm 0.4) \times 10^{-6}$. In contrast, the negative control (*P. protegens*) showed both frequency shift and dissipation change values close to zero: 0.7 ± 0.1 Hz and $(0.9 \pm 0.3) \times 10^{-6}$, respectively, statistically confirming the excellent specificity of the APT1 sensor for *B. subtilis* compared to *P. protegens* (*p*-value 0.0002).

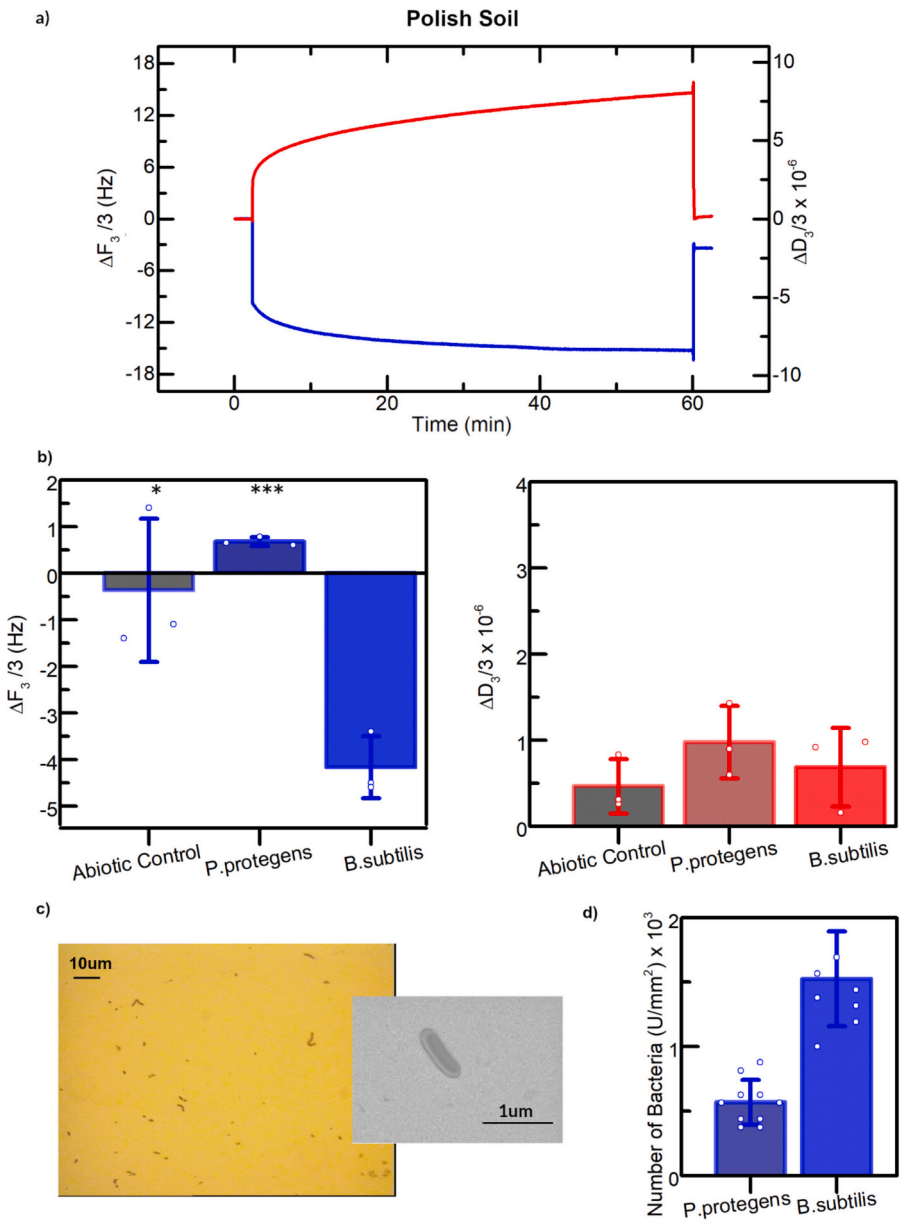

Fig. 4. Detection results for Polish soil**. Panel a)** shows the real-time traces of frequency shift and dissipation in response to *B. subtilis* detection, with a negative frequency shift of approximately −4 Hz and a dissipation change close to zero. **Panel b)** presents the barplot and for each analyzed sample: *B. subtilis*, *P. protegens*, and the abiotic control. The corresponding frequency shift and dissipation change values are reported. Although the number of replicates is limited, the distributions satisfied the normality test, and the data are represented with the mean emphasized. The whiskers indicate the standard deviation. Statistical significance was assessed using a *t*-test, resulting in a *p*-value of 0.02 for the comparison between the frequency shift of the abiotic control and *B. subtilis*, and a p-value of 0.0002 for the comparison between *P. protegens* and *B. subtilis*. **Panel c)** presents a representative image of *B. subtilis* detection, along with an SEM inset illustrating bacterial dimensions. **Panel d)** further summarizes the average bacterial counts per unit area from the analysis, with *B. subtilis* at 1730 U/mm^2 (SD = 500 U/mm^2) and *P. protegens* at 570 U/mm^2 (SD = 160 U/mm^2).

Table 3
Bacteria detection in soils.

	Polish Soil			German Soil		
	P. protegens	*B.subtilis*	*Abiotic*	*P. protegens*	*B. subtilis*	*Abiotic*
$\Delta F_3/3$ [Hz]	0,7 ± 0,1	−4,2 ± 0,5	−0,4 ± 1,3	−7 ± 3	−17 ± 3	−4 ± 1
ΔD_3 /3 [x10^6]	0,9 ± 0,3	0,7 ± 0,4	0,5 ± 0,2	2 ± 2	5 ± 2	1 ± 1

Similarly, the abiotic control (soil extract without inoculation) exhibited an average frequency shift of −0.4 ± 1.3 Hz and a dissipation change of (0.5 ± 0.2) × 10^{-6}, both consistent with the expected near-zero values and significantly different from *B. subtilis* (p-value 0.02). These findings demonstrate that the soil matrix has minimal impact on the QCM-D sensor performance, confirming its ability to maintain high specificity and reliable detection even in the presence of complex environmental samples.

In addition to QCM-D detection results, analysis of the microscopic images further corroborated the high specificity of APT1 and aligned well with the QCM-D results (Fig. 4, panels c,d). On average, approximately three-fold higher numbers of *B. subtilis* cells were counted on the

crystal compared to *P. protegens* (1730 ± 490 U/mm^2 for *B. subtilis* and 570 ± 160 U/mm^2 for *P. protegens*). These microscopy findings strongly support the high specificity of the aptasensor and align well with the QCM-D results, providing comprehensive validation of the sensor's performance in a complex soil matrix.

3.3.5. German soil

The second type of soil tested was a German soil sample. After completing the inoculum preparation and extraction protocol, the bacterial concentration obtained for analysis was approximately 10^7 CFU/ml. The same detection strategy used for the Polish soil was applied.

Fig. 5 presents the detection results for the German soil. Panel a show the real-time traces of frequency shift and dissipation (referred to the 3rd overtone) during *B. subtilis* detection. The traces appear well-defined and exhibit minimal noise, indicating that the soil extract is highly compatible with the QCM-D system.

Panel b, along with Table 3, present the cumulative detection results derived from three replicates, displayed as bar plots to illustrate the mean frequency shifts and dissipation changes for each sample type. For *B. subtilis*, the average frequency shift was −17 ± 3 Hz, accompanied by a dissipation change of (5 ± 2) × 10^{-6}. In contrast, *P. protegens* exhibited a lower frequency shift of −7 ± 3 Hz with a dissipation change of (2 ± 2) × 10^{-6}.

Abiotic control samples yielded an average frequency shift of −4 ± 1 Hz and a dissipation change of (1 ± 1) × 10^{-6}. Although the negative control values were not close to zero, statistical analysis demonstrated that the specificity of APT1 for *B. subtilis* remained significant when compared to both non-inoculated soil (*p*-value 0.0057) and *P. protegens*

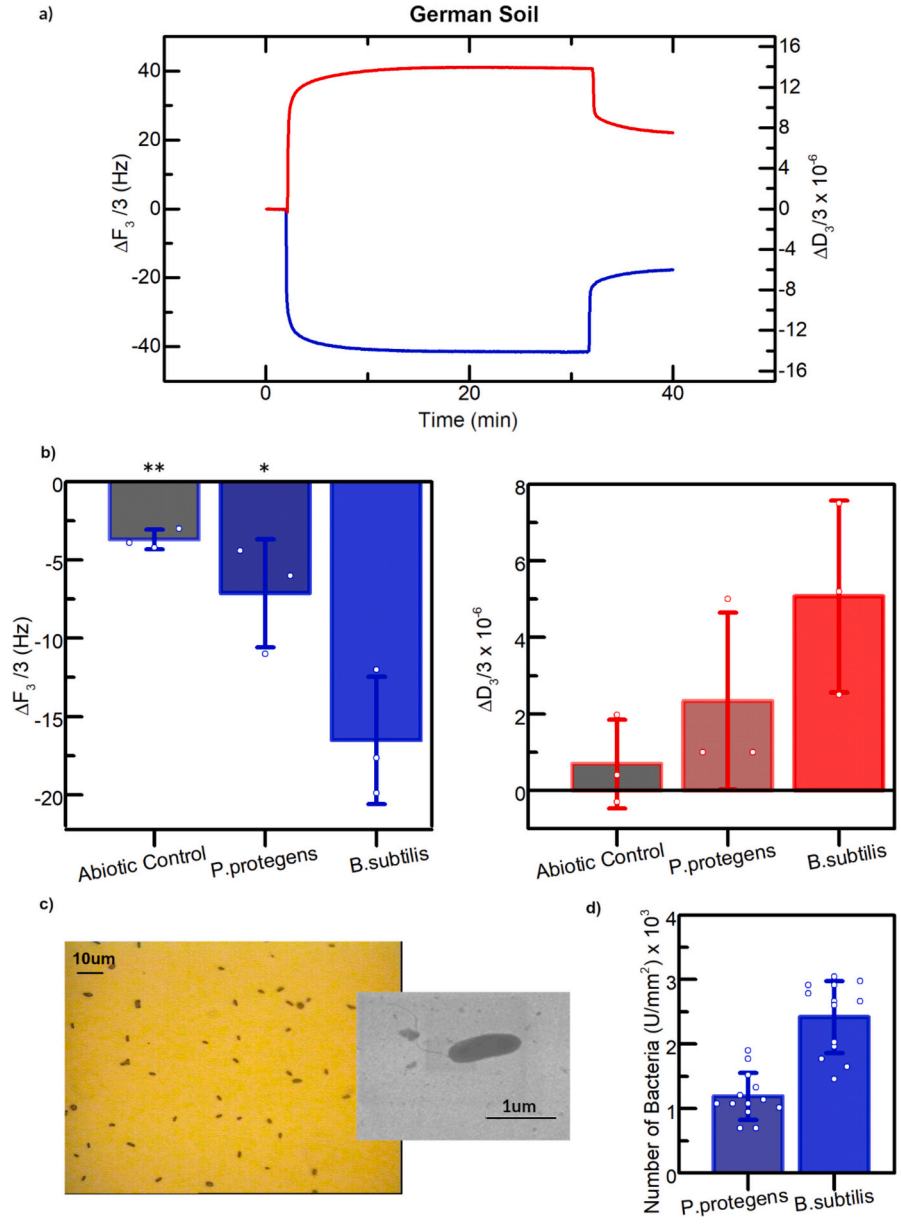

Fig. 5. Detection results for German soil**. Panel a)** shows the real-time traces of frequency shift and dissipation in response to *B. subtilis* detection, with a negative frequency shift of approximately −19 Hz and a dissipation change near to 8 × 10^{-6}. **Panel b)** presents barplots and mean values of replicates for each analyzed sample: *B. subtilis*, *P. protegens*, and the abiotic control. The corresponding frequency shift and dissipation change values are reported. Although the number of replicates is limited, the distributions satisfied the normality test, and the data are represented with the mean emphasized. The whiskers indicate the standard deviation. Statistical significance was assessed using a *t*-test with a *p*-value of 0.04 for the comparison between *P. protegens* and *B. subtilis* **Panel c)** presents a representative image of *B. subtilis* detection, along with an SEM inset illustrating bacterial dimensions. **Panel d)** further summarizes the average bacterial counts per unit area from the analysis, with *B. subtilis* at 2420 U/mm^2 (SD = 540 U/mm^2) and *P. protegens* at 1190 U/mm^2 (SD = 350 U/mm^2).

(p-value 0.04).

To further corroborate the QCM-D results, optical microscopy was employed. Panel c of Fig. 5 shows a representative image of *B. subtilis* binding, complemented by an SEM photo illustrating the bacterial morphology. The bacterial counts per unit area, summarized in panel d of Fig. 5, revealed an average of 2420 ± 540 U/mm^2 for *B. subtilis* and 1190 ± 350 U/mm^2 for *P. protegens*. These microscopy findings align closely with the QCM-D results, reinforcing the aptasensor's strong specificity and reliable performance in complex soil matrices.

4. Discussion

The first aim of this study was to assess the binding affinity and specificity of two different aptamers, APT 1 and APT 2, under controlled conditions in a clean buffer. This comparison allowed the identification of the most reliable candidate for subsequent experiments in complex matrices. Both aptamers demonstrated efficient binding to the sensor surface, as evidenced by distinct negative frequency shifts and minimal dissipation changes, indicating the formation of a rigid and stable binding layer. Regarding AFM morphology, as anticipated, aptamer immobilization increased the negative phase and introduced discrete bright spots, consistent with compact domains or micro-clusters on a continuous matrix. As reported by Takita et al. [33], very thin aptamer layers on gold did not markedly alter AFM morphology. After BSA blocking, filamentous or reticulated features (tens to hundreds of nanometres) appeared, markedly brighter in phase and consistent with densified protein aggregates along preferential pathways, while the background remained a soft organic film. This observation agrees with previous reports [34], confirming a stepwise surface evolution.

However, APT 1 consistently outperformed APT 2 in terms of specificity and reproducibility. APT 1 showed significantly higher binding specificity for *B. subtilis* compared to *P. protegens*, with a clear and statistically significant distinction between positive and negative controls (p-value <0.0001). Conversely, APT 2 exhibited higher variability and lower discrimination capacity, particularly when detecting *B. subtilis* in the presence of potential interfering species. These findings led to the selection of APT 1 for subsequent experiments involving more complex matrices. This result is in line with the findings of the preliminary study by Manfredini et al., where these two types of aptamers were synthesized and tested for the first time [10].

Additionally, the strong correlation observed between QCM-D and optical microscopy results for both aptamers highlights the robustness of the combined approach, as the frequency shift directly correlates with the adhered bacterial mass. This complementary validation strengthens the reliability of the QCM-D signals, as evidenced by the high statistical significance (p-value <0.0001) obtained when comparing both *B. subtilis* to *P. protegens* and the mixed bacteria sample to *P. protegens*.

Despite the overall consistency between the two methodologies, a marked difference emerged between APT 1 and APT 2 in terms of data variability. While APT 1 demonstrated consistent and reproducible results, APT 2 exhibited significantly higher variability, particularly in *B. subtilis* samples. This variability could arise from non-specific interactions or heterogeneous binding, which not only affects the accuracy of bacterial counting but also reduces the strength of correlation with the QCM-D results.

Once APT 1 was established as the superior aptamer, the system was tested in complex soil matrices to evaluate its real-world applicability. We used three soils differing in their main physico-chemical parameters, which are known to influence the persistence of microorganisms: organic matter content, pH, and texture. Specifically, we investigated detection in a sandy soil with neutral pH from Poland and a medium-textured sandy loam soil with sub-alkaline pH from Germany.

The release of bacteria from soil particles and aggregates is a vital step in evaluating the microbial population within the soil. This stage is where considerable variation in the recovery of viable bacteria can arise. The main goal was to maximize bacterial extraction efficiency to reduce quantification errors during subsequent QCM-D aptasensor analysis.

The calculated persistence rates were 74.4 % for *B. subtilis* and 80 % for *P. protegens* in Polish soil, while in German soil the rates were 58.8 % and 73.3 %, respectively. These results indicate that both soil types supported bacterial persistence, with Polish soil demonstrating slightly higher recovery rates, suggesting better retention and viability conditions for the target organisms.

The choice to assess the performance of the aptasensor at a bacterial concentration of 10^6 CFU/ml is well-aligned with the concentrations typically found in *B. subtilis*-based biofertilizers, approximately 10^8 CFU/ml. There is experimental evidence showing that, after inoculating the soil with *B. subtilis*, the bacterial population in the rhizosphere (the narrow region of soil directly influenced by plant roots) remained stable at approximately 10^8 CFU per gram of dry rhizosphere soil for one month. [35] Considering the extraction method using 2 g of soil and 8 ml of extracting solution, a value of 10^8 CFU/g corresponds to approximately 2.5×10^7 CFU/ml in the extracting solution. The outcomes obtained at a concentration of 10^5 CFU/ml enable the determination of a limit of detection LoD for the experimental platform between 10^5 and 10^6 CFU/ml, which is compatible with applications involving the monitoring of biofertilizers in soil.

The preparation of the soil-derived liquid phase was a critical aspect of this study, as it directly influenced the compatibility of the sample with the QCM-D microfluidic system. The extraction method was optimized to produce a clear, sediment-free liquid phase by focusing on sedimentation behavior and physicochemical characterization. An extract with reduced turbidity and fewer large particles proved particularly suitable for use in QCM-D microfluidic studies, minimizing the risk of nonspecific deposition of large particles on the crystal surface. Moreover, the elution buffer was selected for its proven efficacy in detaching microbial cells from soil particles. Sodium pyrophosphate acts as a dispersing agent by chelating divalent cations (Ca^{2+}, Mg^{2+}) that stabilize soil aggregates, thereby weakening electrostatic interactions between particles and cells. Tween 20, a non-ionic surfactant, further reduces surface tension and disrupts hydrophobic interactions between bacterial membranes and soil organic matter. The combined action of these two agents facilitates efficient desorption of bacteria from soil particles while preserving cell integrity, ensuring consistent and reproducible recovery across different soil types.

These findings demonstrate the importance of optimizing extraction protocols to achieve optical clarity and minimizing scattering, thereby enhancing the reliability of the QCM-D detection system.

UV–Vis spectrophotometric analysis further confirmed the effectiveness of the sedimentation method, revealing that the resulting extract is markedly clearer and exhibits a sharp decline in absorption after 400 nm. This behavior indicates the removal of particles and chromophores associated with the precipitated fraction, thereby confirming the suitability of the extraction process for producing a clean and compatible sample for QCM-D analysis.

The QCM-D analysis of soil samples demonstrated robust performance of the aptasensor, even in the presence of complex soil matrices. Both Polish and German soil extracts were analyzed, and the results confirmed the sensor's ability to maintain high specificity and reliable detection. In Polish soil, *B. subtilis* was successfully detected with a mean frequency shift of −4.2 ± 0.5 Hz, while *P. protegens* and abiotic controls showed frequency shifts close to zero, highlighting the excellent specificity of the aptasensor in this matrix (p-value = 0.0002). Similarly, in German soil samples, the sensor maintained reliable performance despite the more challenging matrix conditions, demonstrating a frequency shift of −17 ± 3 Hz for *B. subtilis* compared to −7 ± 3 Hz for *P. protegens*, with significant differences between positive and negative controls (p-value = 0.04).

In both cases, despite the negative control values not being close to zero, statistical analysis confirmed the sensor's specificity, with significant p-values. This demonstrates that the aptasensor's detection capability is not compromised by the inherent complexity of the soil extract.

These findings confirm that the optimized QCM-D system is suitable for detecting bacterial contamination in diverse and complex soil environments.

The higher control values and elevated dissipation changes observed in the German soil samples can likely be attributed to the more complex composition of the loam soil matrix. Loam soils generally contain more nutrients, moisture, and humus, which may contribute to these effects. Furthermore, the high dissipation change value obtained for *B. subtilis* in the German soil is consistent with literature data, suggesting a dissipation effect and a transition to a viscoelastic regime due to the high mass adhesion on the sensor. [36].

Furthermore, the strong agreement between QCM-D detection and microscopic analysis for both Polish and German soil samples reinforce the robustness and reliability of the aptasensor. In the Polish soil matrix, the three-fold higher number of *B. subtilis* cells observed microscopically compared to *P. protegens* further highlights the high specificity of the sensor, aligning well with the QCM-D results. Similarly, the high consistency between QCM-D detection and optical microscopy analysis for German soil samples demonstrates the robustness of the aptasensor, even in the presence of a complex environmental matrix.

In scientific literature, several studies have demonstrated the potential of combining QCM-D systems with aptamer-based functionalization for bacterial detection. Reported detection limits range from 10^2 to 10^7 CFU/ml, which is consistent with the performance obtained in the present study. Notably, Yu et al. demonstrated the use of a QCM-D aptasensor to detect *E. coli* with a limit of detection (LOD) of 1.46×10^3 CFU/ml, showcasing the technique's sensitivity and speed [37]. Similarly, V.C. Ozalp et al. applied a QCM-D sensor functionalized with aptamers to detect *Salmonella* in milk samples, highlighting the capability of this technology to perform in complex matrices. [38].

In this study, the performance of QCM-D crystals was tested immediately after functionalization, without investigating thermal and chemical stability in terms of long-term shelf life of the functionalization. However, several reports in the literature on aptasensors confirm the robustness of aptamer-based functionalization, as for instance in the work of Domsicova et al. [39], where the stability of the aptasensor was tested and validated with clinical patient samples, marking an important step toward real clinical application. In addition, as highlighted in the work of Manfredini et al. [10], ssDNA aptamers exhibit high thermal and chemical stability, being resistant to degradation and easily amenable to chemical modification and immobilization. These intrinsic features make them particularly suitable for the design of point-of-care devices based on pre-functionalized sensitive elements, such as QCM crystals.

Compared to conventional detection methods such as microbial culturing, quantitative PCR (qPCR), and genomic hybridization, the QCM-D-based aptasensor developed in this study offers distinct advantages. While culturing methods are time-consuming and require long incubation periods, the QCM-D aptasensor enables rapid and real-time detection. Similarly, although qPCR and genomic hybridization are highly sensitive, they demand sophisticated laboratory equipment and expertise, as well as extensive sample preparation steps that are not easily adaptable to field applications. In contrast, the QCM-D-based aptasensor demonstrated in this study provides near real-time detection with high specificity and compatibility with chemically complex matrices like soil.

5. Conclusion

This study successfully demonstrates the applicability and robustness of a QCM-D aptasensor functionalized with two distinct aptamers, APT 1 and APT 2, for detecting *B. subtilis*. The detection of samples is achieved through monitoring the resonance frequency of the QCM-D, which highlights the high affinity and reproducibility of the bacteria on the crystal surface.

In buffer, both aptamers performed effectively, but APT 1 exhibited superior selectivity and specificity ($p = 0.019$). This distinction led to its selection for soil analyses, consistent with previous findings on its strong binding affinity for *B. subtilis* strains. The QCM-D sensor, tested at concentrations aligning with practical applications for biofertilizer monitoring, demonstrated a limit of detection (LoD) between 10^5 and 10^6 CFU/ml, suitable for field-relevant concentrations.In soil matrices, APT 1 consistently enabled the reliable detection of *B. subtilis*, showing a strong correlation between image-based bacterial counts and QCM-D frequency shifts. Polish soil samples closely paralleled the results from clean buffer, underscoring the sensor's specificity and limited interference from the soil matrix. The German soil samples, while presenting additional complexity and viscoelastic behavior, nonetheless permitted significant distinctions between *B. subtilis* and controls, reaffirming the aptasensor's versatility across varied soil types. Statistical analysis validates specificity across soils ($p = 0.0002$ in Polish soil; $p = 0.04$ in German soil). Microscopy corroborates these findings, revealing approximately three-fold higher *B. subtilis* cell counts compared to *P. protegens*.

To the best of our knowledge, this is the first QCM-D–based aptasensor reported for the detection of a bacterial inoculant in soil. The functionalization with APT 1 provides a promising platform for the selective and sensitive detection of *B. subtilis* in both controlled and complex soil environments. Moreover, we developed an extraction technique capable of producing a sample compatible with the microfluidics of the sensor platform, yielding recovery rates of ~72 % and ensuring suitability for field applications. As previously anticipated, the results obtained in terms of LoD, rapidity, and simplicity of detection are consistent with those reported in the literature on QCM aptasensors for bacterial detection.

As already mentioned in introduction, regarding the field of *monitoring of bioinoculants in soil*, the most innovative methods described in the last years mainly rely on real-time polymerase chain reaction (qPCR). For instance, the work of Iosa et al. developed a qPCR protocol for the species-specific quantification of plant growth-promoting rhizobacteria (PGPR) in agricultural soils. This study provides a rapid evaluation of large-scale field experiments (as opposed to traditional culturing methods) and ensures a reliable monitoring of PGPR presence up to one month after inoculation. [40].

In the field of plant pathogen detection, the review *"Portable solutions for plant pathogen diagnostics: development, usage, and future potential"* highlights that the most significant technological innovations can be grouped into (in addition to nucleic acid amplification methods) electrochemical, optical, and immunoassay-based approaches (such as ELISA and lateral flow assays) [41]. These strategies have significantly contributed to the development of portable diagnostic tools, aiming to provide more accessible, user-friendly, and rapid solutions for pathogen detection in agricultural settings.

Compared to those approaches, our work introduces a gravimetric sensing method (QCM-D) coupled with specific aptamers, which offers several complementary advantages. First, QCM-D is a label-free technology, providing real-time detection of binding events without the need for fluorescent probes, enzymes, or amplification reagents. This reduces both the complexity of the assay and the costs associated with consumables, maintaining excellent reproducibility. Second, QCM-D is inherently versatile: beyond simply detecting the presence of bioinoculants, it can provide information on the viscoelastic properties of attached layers. Finally, with the growing commercial availability of portable QCM devices, this technology can be envisioned as a practical *on field tool* for monitoring in precision agriculture.

This makes it highly promising for *in-field applications*, where the combination of simplicity, rapid response, and cost-effectiveness is essential. By integrating these features, our approach can expand the toolbox of portable diagnostic solutions, offering an alternative path alongside electrochemical, optical, and immunoassay platforms. To fully realize this potential, extraction and detection times should be optimized, and functionalization and sample preparation strategies adapted for portable QCM systems [42] or other acoustic wave devices, such as

SAW sensors [43]. Ultimately, the development of portable and robust systems that maintain high sensitivity and specificity while minimizing analysis time will be essential for enabling practical on-site applications. In the perspective of future on-field applications, it will be essential to investigate the long-term stability of the functionalized sensors and to establish optimal storage strategies to preserve their functionality throughout time. The present aptasensor can also be applied to monitor the shelf life of bio-based products, ensuring quality and effectiveness over time. Furthermore, persistence tracking can allow farmers and manufacturers to improve product performance. These aspects may also support documentation required for registration and provide tools for regulatory bodies tasked with controlling and preventing fraud in the development and use of microorganism-based formulations.

CRediT authorship contribution statement

Francesco Lunardelli: Writing – original draft, Visualization, Validation, Software, Methodology, Investigation, Formal analysis, Data curation. **Andrea Manfredini:** Writing – review & editing, Methodology, Investigation, Formal analysis, Data curation. **Loredana Canfora:** Writing – review & editing, Supervision, Methodology, Investigation, Conceptualization. **Mariacristina Gagliardi:** Writing – review & editing, Methodology, Investigation, Conceptualization. **Matteo Agostini:** Writing – review & editing, Funding acquisition, Conceptualization. **Domenica Convertino:** Writing – review & editing, Formal analysis, Data curation. **Stefano Mocali:** Writing – review & editing, Methodology, Conceptualization. **Eligio Malusa:** Writing – review & editing, Supervision, Funding acquisition, Conceptualization. **Marco Cecchini:** Writing – review & editing, Visualization, Validation, Supervision, Resources, Methodology, Funding acquisition, Formal analysis, Data curation, Conceptualization.

Declaration of competing interest

The authors declare the following financial interests/personal relationships which may be considered as potential competing interests: Marco Cecchini reports financial support was provided by European Union. Eligio Malusa reports financial support was provided by European Union. Stefano Mocali reports financial support was provided by European Union. Marco Cecchini reports a relationship with INTA srl that includes: equity or stocks. Matteo Agostini reports a relationship with INTA srl that includes: board membership, employment, and equity or stocks. Loredana Canfora has patent #EU patent application EP4365292 pending to Consiglio Per La Ricerca In Agricoltura E L'analisi Dell'economia Agraria. Manfredini Andrea has patent #EU patent application EP4365292 pending to Consiglio Per La Ricerca In Agricoltura E L'analisi Dell'economia Agraria. Eligio Malusa has patent #EU patent application EP4365292 pending to Consiglio Per La Ricerca In Agricoltura E L'analisi Dell'economia Agraria. Stefano Mocali has patent #EU patent application EP4365292 pending to Consiglio Per La Ricerca In Agricoltura E L'analisi Dell'economia Agraria. If there are other authors, they declare that they have no known competing financial interests or personal relationships that could have appeared to influence the work reported in this paper.

Acknowledgements

This research was performed under the EXCALIBUR project, funded by the European Union's Horizon 2020 Research and Innovation Program (Grant Agreement No. 817946), and under the SPIN-FERT project, funded by the European MISSION SOIL Innovation Action Program (Grant Agreement No. 101157265).

Appendix A. Supplementary data

Supplementary data to this article can be found online at https://doi.org/10.1016/j.microc.2025.116112.

Data availability

Data are avialable on the Zenodo Platform (DOI: 10.5281/zenodo.15073745)

References

[1] D. Das, S. Sengupta, The role of microorganisms in agriculture: enhancing soil health, crop productivity, and sustainable farming practices, Int. J. Agric. Food Sci. 6 (2) (2024) 163–165, https://doi.org/10.33545/2664844X.2024.v6.i2c.219.
[2] E. Malusà, F. Pinzari, L. Canfora, Efficacy of biofertilizers: Challenges to improve crop production, in: D. Singh, H. Singh, R. Prabha (Eds.), Microbial Inoculants in Sustainable Agricultural Productivity, Springer, New Delhi, 2016, pp. 17–40, https://doi.org/10.1007/978-81-322-2644-4_2.
[3] J. Wesseler, The EU'S farm-to-fork strategy: an assessment from the perspective of agricultural economics, Appl. Econ. Perspect. Policy 44 (4) (2022) 1826–1843, https://doi.org/10.1002/aepp.13239.
[4] E. Malusà, G. Berg, A. Biere, A. Bohr, L. Canfora, A.D. Jungblut, et al., A holistic approach for enhancing the efficacy of soil microbial inoculants in agriculture: from lab to field scale, Global J. Agricultural Innovation Res. Develop. 8 (2021) 176–190, https://doi.org/10.15377/2409-9813.2021.08.14.
[5] A. Manfredini, E. Malusà, C. Costa, F. Pallottino, S. Mocali, F. Pinzari, et al., Current methods, common practices, and perspectives in tracking and monitoring bioinoculants in soil, Front. Microbiol. 12 (2021) 698491, https://doi.org/10.3389/fmicb.2021.698491.
[6] G. Venbrux, B. De Baets, W. Waegeman, Current and emerging trends in techniques for plant pathogen detection, Front. Plant Sci. 14 (2023) 1120968, https://doi.org/10.3389/fpls.2023.1120968.
[7] R. Zia, M. Iftikhar, A. Rafiq, S. Hakim, M.S. Nawaz, A. Imran, S.Z. Bajwa, Nanosensors for microbial detection in soil, in: A. Denizli, T.A. Nguyen, S. Rajendran, G. Yasin, A.K. Nadda (Eds.), Nanosensors for Smart Agriculture. Micro and Nano Technologies, Elsevier, Amsterdam, 2022, pp. 367–400, https://doi.org/10.1016/B978-0-12-824554-5.00003-3.
[8] V.J. Gadkar, M. Filion, Quantitative real-time polymerase chain reaction for tracking microbial gene expression in complex environmental matrices, Curr. Issues Mol. Biol. 15 (2) (2013) 45–58, https://doi.org/10.21775/cimb.015.045.
[9] T. Van Rossum, P. Ferretti, O.M. Maistrenko, P. Bork, Diversity within species: interpreting strains in microbiomes, Nat. Rev. Microbiol. 18 (9) (2020) 491–506, https://doi.org/10.1038/s41579-020-0368-1.
[10] A. Manfredini, E. Malusà, L. Canfora, Aptamer-based technology for detecting Bacillus subtilis in soil, Appl. Microbiol. Biotechnol. 107 (22) (2023) 6963–6972, https://doi.org/10.1007/s00253-023-12765-0.
[11] U. Azizoglu, *Bacillus thuringiensis* as a biofertilizer and biostimulator: a Mini-review of the little-known plant growth-promoting properties of *Bt*, Curr. Microbiol. 76 (2019) 1379–1385, https://doi.org/10.1007/s00284-019-01705-9.
[12] A.K. Saxena, M. Kumar, H. Chakdar, N. Anuroopa, D.J. Bagyaraj, *Bacillus* species in soil as a natural resource for plant health and nutrition, J. Appl. Microbiol. 128 (6) (2020) 1583–1594, https://doi.org/10.1111/jam.14506.
[13] S. Mahapatra, R. Yadav, W. Ramakrishna, Bacillus subtilis impact on plant growth, soil health and environment: Dr. Jekyll and Mr. Hyde, J. Appl. Microbiol. 132 (5) (2022) 3543–3562, https://doi.org/10.1111/jam.15480.
[14] R. Fogel, J. Limson, A.A. Seshia, Acoustic biosensors, Essays Biochem. 60 (1) (2016) 101–110, https://doi.org/10.1042/EBC20150011.
[15] K. Sakai, Quartz crystal microbalance with dissipation monitoring (QCM-D), in: M. Abe (Ed.), Measurement Techniques and Practices of Colloid and Interface Phenomena, Springer, Singapore, 2019, https://doi.org/10.1007/978-981-13-5931-6_7.
[16] G. Sauerbrey, Verwendung von Schwingquarzen zur Wägung dünner Schichten und zur Mikrowägung, Z. Phys. 155 (1959) 206–222, https://doi.org/10.1007/BF01337937.
[17] M.V. Voinova, M. Rodahl, M. Jonson, B. Kasemo, Viscoelastic acoustic response of layered polymer films at fluid-solid interfaces: continuum mechanics approach, Phys Scr 59 (5) (1999) 391–396, https://doi.org/10.1238/Physica.Regular.059a00391.
[18] M. Gagliardi, G. Tori, M. Agostini, F. Lunardelli, F. Mencarelli, C. Sanmartin, M. Cecchini, Detection of oenological polyphenols via QCM-D measurements, Nanomaterials (Basel) 12 (1) (2022) 166, https://doi.org/10.3390/nano12010166.
[19] S. Akgönüllü, E. Özgür, A. Denizli, Quartz crystal microbalance-based Aptasensors for medical diagnosis, Micromachines 13 (2022) 1441, https://doi.org/10.3390/mi13091441.
[20] M. Agostini, F. Amato, M.L. Vieri, G. Greco, I. Tonazzini, L. Baroncelli, et al., Glial-fibrillary-acidic-protein (GFAP) biomarker detection in serum-matrix: functionalization strategies and detection by an ultra-high-frequency surface-acoustic-wave (UHF-SAW) lab-on-chip, Biosens. Bioelectron. 172 (2020) 112774, https://doi.org/10.1016/j.bios.2020.112774.
[21] S. Akgönüllü, E. Özgür, A. Denizli, Recent advances in quartz crystal microbalance biosensors based on the molecular imprinting technique for disease-related biomarkers, Chemosensors 10 (2022) 106, https://doi.org/10.3390/chemosensors10030106.

[22] M. Andersson, J. Andersson, A. Sellborn, M. Berglin, B. Nilsson, H. Elwing, Quartz crystal microbalance-with dissipation monitoring (QCM-D) for real time measurements of blood coagulation density and immune complement activation on artificial surfaces, Biosens. Bioelectron. (2005) 21(1), https://doi.org/10.1016/j.bios.2004.09.026.

[23] U.S. Kadam, J.C. Hong, Advances in aptameric biosensors designed to detect toxic contaminants from food, water, human fluids, and the environment, Trends Environ Anal Chem. 36 (2022) e00184, https://doi.org/10.1016/j.teac.2022.e00184.

[24] A. Azzouz, V. Kumar, L. Hejji, K.H. Kim, Advancements in nanomaterial-based aptasensors for the detection of emerging organic pollutants in environmental and biological samples, Biotechnol. Adv. 66 (2023) 108156, https://doi.org/10.1016/j.biotechadv.2023.108156.

[25] X. Li, Y. Zhang, Nanomaterial-based aptasensors for environmental monitoring, Curr. Opin. Environ. Sci. Health. 11 (2019) 1–8, https://doi.org/10.1016/j.coesh.2019.09.003.

[26] M.Y. Song, D. Nguyen, S.W. Hong, B.C. Kim, Broadly reactive aptamers targeting bacteria belonging to different genera using a sequential toggle cell-SELEX, Sci. Rep. 7 (2017) 43641, https://doi.org/10.1038/srep43641.

[27] M. Zuker, Mfold web server for nucleic acid folding and hybridization prediction, Nucleic Acids Res. 31 (13) (2003) 3406–3415, https://doi.org/10.1093/nar/gkg595.

[28] G. Tóth, A. Jones, L. Montanarella, The LUCAS topsoil database and derived information on the regional variability of cropland topsoil properties in the European Union, Environ. Monit. Assess. 185 (9) (2013) 7409–7425, https://doi.org/10.1007/s10661-013-3109-3.

[29] J. Kobel-Boelke, B. Tienken, A. Nehrkorn, Microbial communities in the saturated groundwater environment. I: methods of isolation and characterization of heterotrophic bacteria, Microb. Ecol. 16 (1988) 17–29.

[30] T. Kakiuchi, M. Iida, S. Imabayashi, K. Niki, Miscibility of adsorbed 1-undecanethiol and 11-mercaptoundecanoic acid species in binary self-assembled monolayers on au(111), Langmuir 17 (5) (2001) 1599–1603, https://doi.org/10.1021/la0014757.

[31] H.B. Pyo, Y.B. Shin, M.G. Kim, H.C. Yoon, Surface plasmon resonance imaging studies for proteolytic hydrolysis of proteins, Langmuir 21 (1) (2005) 166–172, https://doi.org/10.1021/la0486382.

[32] M.R. Lockett, M.F. Phillips, J.L. Jarecki, D. Peelen, L.M. Smith, A tetrafluorophenyl activated ester self-assembled monolayer for the immobilization of amine-modified oligonucleotides, Langmuir 24 (1) (2008) 69–75, https://doi.org/10.1021/la702493u.

[33] S. Takita, A. Nabok, A. Lishchuk, M.H. Mussa, D. Smith, Enhanced performance electrochemical biosensor for detection of prostate Cancer biomarker PCA3 using specific aptamer, Eng 4 (2023) 367–379, https://doi.org/10.3390/eng4010022.

[34] V. Vetri, M. D'Amico, V. Foderà, M. Leone, A. Ponzoni, G. Sberveglieri, V. Militello, Bovine serum albumin protofibril-like aggregates formation: solo but not simple mechanism, Arch. Biochem. Biophys. 508 (2011) 13–24, https://doi.org/10.1016/j.abb.2011.01.024.

[35] Q. Zhao, Q. Shen, W. Ran, T. Xiao, D. Xu, Y. Xu, Inoculation of soil by *Bacillus subtilis* Y-IVI improves plant growth and colonization of the rhizosphere and interior tissues of muskmelon (*Cucumis melo* L.), Biol. Fertil. Soils 47 (5) (2011) 507–514, https://doi.org/10.1007/s00374-011-0558-0.

[36] M. Tatarko, S. Spagnolo, V. Oravczová, J. Süle, M. Hun, A. Hucker, T. Hianik, Changes of viscoelastic properties of aptamer-based sensing layers following interaction with *listeria innocua*, Sensors (Basel). 21 (16) (2021) 5585, https://doi.org/10.3390/s21165585.

[37] X. Yu, F. Chen, R. Wang, Y. Li, Whole-bacterium SELEX of DNA aptamers for rapid detection of *E. coli* O157:H7 using a QCM sensor, J. Biotechnol. 266 (2018) 39–49, https://doi.org/10.1016/j.jbiotec.2017.12.011.

[38] V.C. Ozalp, G. Bayramoglu, Z. Erdem, M.Y. Arica, Pathogen detection in complex samples by quartz crystal microbalance sensor coupled to aptamer functionalized core–shell type magnetic separation, Anal. Chim. Acta 853 (2015) 533–540, https://doi.org/10.1016/j.aca.2014.10.010.

[39] Michaela Domsicova, Simona Kurekova, Andrea Babelova, Kristina Jakic, Iveta Oravcova, Veronika Nemethova, Filip Razga, Albert Breier, Miroslav Gal, Alexandra Poturnayova, Advancements in chronic myeloid Leukemia detection: development and evaluation of a novel QCM aptasensor for use in clinical practice, Biochem. Biophys. Rep. 39 (2024) 101816, https://doi.org/10.1016/j.bbrep.2024.101816.

[40] I. Iosa, C. Agrimonti, N. Marmiroli, Real-time PCR (qtPCR) to discover the fate of plant growth-promoting rhizobacteria (PGPR) in agricultural soils, Microorganisms 12 (5) (2024) 1002, https://doi.org/10.3390/microorganisms12051002.

[41] A. Yadav, K. Yadav, Portable solutions for plant pathogen diagnostics: development, usage, and future potential, Front. Microbiol. 16 (2025), https://doi.org/10.3389/fmicb.2025.1516723.

[42] R.J. Horst, A. Katzourakis, B.T. Mei, S. de Beer, Design and validation of a low-cost open-source impedance based quartz crystal microbalance for electrochemical research, HardwareX 12 (2022) e00374, https://doi.org/10.1016/j.ohx.2022.e00374.

[43] M. Gagliardi, M. Agostini, F. Lunardelli, L. Lamanna, A. Miranda, A. Bazzichi, A. G. Luminare, F. Cervelli, F. Gambineri, M. Totaro, M. Lai, G. Maisetta, G. Batoni, M. Pistello, M. Cecchini, Surface acoustic wave-based lab-on-a-chip for the fast detection of *legionella pneumophila* in water, Sensors Actuators B Chem. 379 (2023) 133299, https://doi.org/10.1016/j.snb.2023.133299.